Volume 11
Number 5
7 February 2023
Pages 927–1162

Journal of Materials Chemistry B

Materials for biology and medicine

rsc.li/materials-b

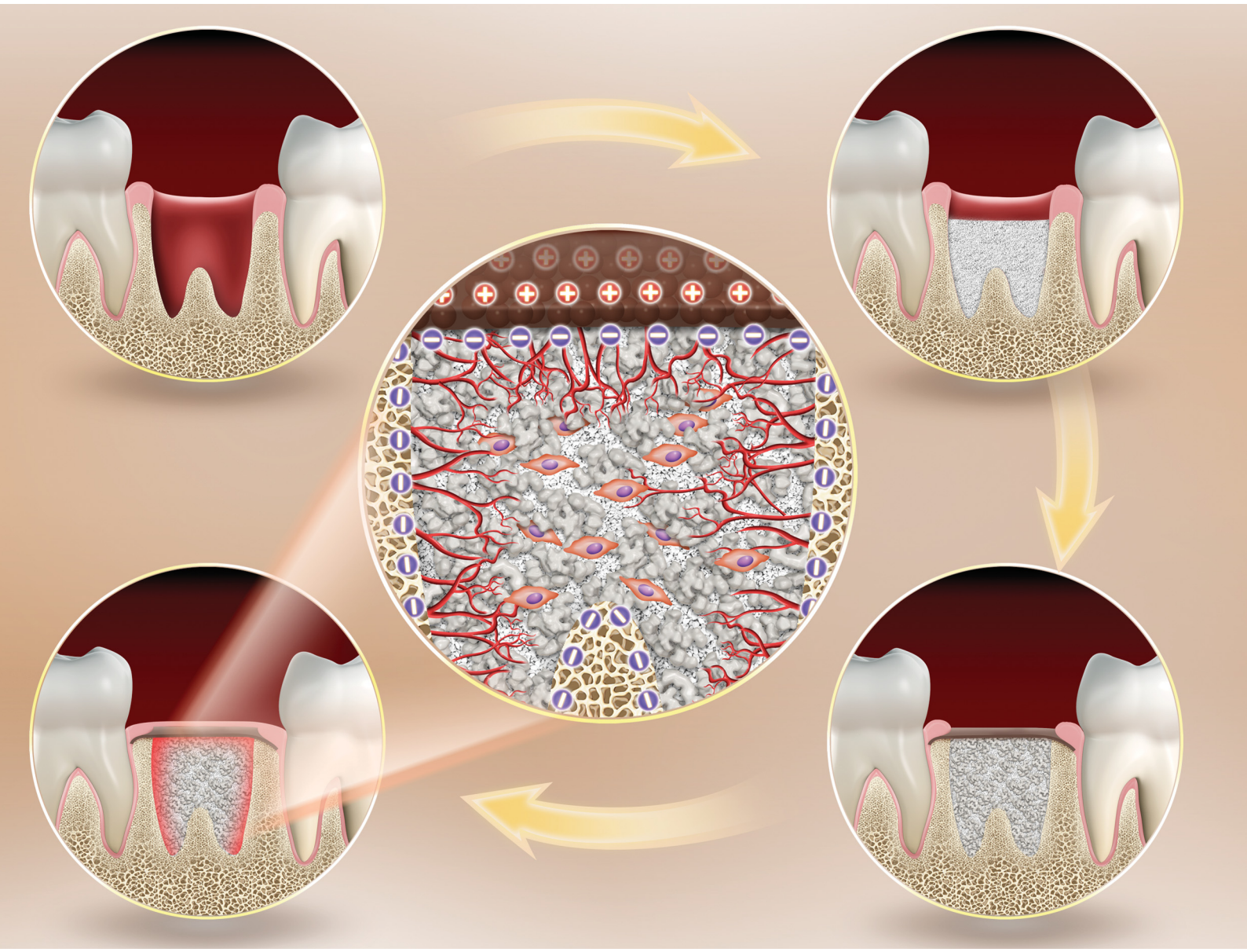

ISSN 2050-750X

ROYAL SOCIETY OF CHEMISTRY

PAPER

Min Gao, Xiaona Zheng, Xuehui Zhang *et al.*
Restoring the electrical microenvironment using ferroelectric nanocomposite membranes to enhance alveolar ridge regeneration in a mini-pig preclinical model

10 YEARS ANNIVERSARY

Journal of Materials Chemistry B

ROYAL SOCIETY OF CHEMISTRY

PAPER

View Article Online
View Journal | View Issue

Cite this: J. Mater. Chem. B, 2023, 11, 985

Restoring the electrical microenvironment using ferroelectric nanocomposite membranes to enhance alveolar ridge regeneration in a mini-pig preclinical model†

Yiping Li,‡[abc] Yanze Meng,‡[a] Yunyang Bai,‡[c] Yijun Wang,‡[a] Jiaqi Wang,‡[b] Boonchin Heng,[d] Jinqi Wei,[e] Xi Jiang,[f] Min Gao,*[cg] Xiaona Zheng,*[cg] Xuehui Zhang *[ag] and Xuliang Deng[cg]

The maintenance and incremental growth of the alveolar bone at the tooth extraction site, to achieve the required height and width for implant restoration, remains a major clinical challenge. Here, the concept of restoring the electrical microenvironment to improve the effects of alveolar ridge preservation (ARP) was investigated in a mini-pig preclinical model. The endogeneous electrical microenvironment of the dental alveolar socket was recapitulated by fabricating a biomimetic ferroelectric $BaTiO_3$/poly(vinylidene fluoridetrifluoroethylene) (BTO/P(VDF-TrFE)) non-resorbable nanocomposite membrane polarized by corona poling. The polarized nanocomposite membrane exhibited excellent electrical stability. After implantation with bone grafts and covering with the charged membrane in tooth extraction sites for three months, both the vertical and horizontal dimension resorption of the alveolar ridge were significantly prevented, as assessed by cone beam computed tomography (CBCT) analyses. Micro-CT analysis showed that the charged membrane induced significant enhancement of newly regenerated bone at the tooth extraction sites. Histological analysis further confirmed that the restoration of the electrical microenvironment significantly promoted buccal alveolar bone regeneration and maturation. In addition, the charged membranes can maintain their structural integrity during the entire implantation period and exhibit positive long-term systemic safety, as assessed by preclinical sub-chronic systemic toxicity. These findings thus provide an innovative strategy for restoring the electrical microenvironment to enhance ARP following dentition defect and edentulism, which could further advance prosthodontics implant technology.

Received 27th September 2022,
Accepted 29th November 2022

DOI: 10.1039/d2tb02054h

rsc.li/materials-b

Introduction

In oral implantology, the maintenance and incremental growth of the alveolar bone at the implantation site are essential prerequisites for achieving long-term optimal functional and aesthetic results. Various therapeutic modalities for alveolar ridge preservation (ARP) have been investigated to reduce bone resorption after tooth extraction and facilitate subsequent implant-supported restoration.[1–4] Therefore, the optimization of ARP will be a major breakthrough in implantology.

During ARP, bone-filling grafts and barrier membranes are routinely used for the treatment of tooth extraction sites, and have demonstrated partial efficacy in preserving the residual alveolar ridge.[5] Resorbable membranes are usually preferred as this would obviate the need for additional surgery to remove the membrane after healing.[6] Nevertheless, non-resorbable membranes are better able to maintain their protective barrier function until their removal.[7,8] To date, many studies have demonstrated that non-resorbable membranes always yield

[a] Department of Dental Materials & Dental Medical Devices Testing Center, Peking University School and Hospital of Stomatology, Beijing, 100081, P. R. China. E-mail: zhangxuehui@bjmu.edu.cn
[b] Department of Prosthodontics, Xiangya Stomatological Hospital & School of Stomatology, Central South University, Changsha, 410078, P. R. China
[c] Department of Geriatric Dentistry, Peking University School and Hospital of Stomatology, Beijing, 100081, P. R. China. E-mail: zhengxiaona@pku.edu.cn, dzgaomin@163.com
[d] Central Laboratory, Peking University School and Hospital of Stomatology, Beijing, 100081, P. R. China
[e] First Clinical Division, Peking University School and Hospital of Stomatology, Beijing, 100081, P. R. China
[f] Department of Oral Implantology, Peking University School and Hospital of Stomatology, Beijing, 100081, P. R. China
[g] National Engineering Research Center of Oral Biomaterials and Digital Medical Devices, NMPA Key Laboratory for Dental Materials, Beijing Laboratory of Biomedical Materials & Beijing Key Laboratory of Digital Stomatology, Peking University School and Hospital of Stomatology, Beijing 100081, P. R. China

† Electronic supplementary information (ESI) available. See DOI: https://doi.org/10.1039/d2tb02054h

‡ These authors contributed equally to this work.

better outcomes for large bone defect areas, as compared to resorbable membranes.[9,10] Nevertheless, non-resorbable membranes often compromise osteogenesis because of the lack of adequate osteoinductivity, which greatly limits subsequent implant restoration therapy. Therefore, based on the intrinsic characteristics of the alveolar bone in the extraction socket, designing an innovative non-resorbable membrane material with improved osteoinductive properties might be an effective strategy to improve the therapeutic efficacy of ARP.

It has been proposed that physiological endogenous electric fields or electrical potential existing within injured tissues play a critical role in the wound healing process[11,12] and bone regeneration.[13] Inspired by this naturally-occurring phenomenon, numerous studies have attempted to recapitulate the physiological electrical microenvironment through the fabrication of various electroactive biomaterials. We had previously conducted studies to prove the concept that ferroelectric nanocomposite membranes comprising $BaTiO_3$ (BTO) nanoparticle fillers and a poly(vinylidene fluoridetrifluoroethylene) (P(VDF-TrFE)) matrix with a biomimetic surface potential can promote rapid bone regeneration by restoring the physiological electrical microenvironment.[14,15] The extraction socket formed after tooth extraction is actually equivalent to an alveolar bone defect. Therefore, the electrical microenvironment of the alveolar bone in the extraction socket may play an important role in alveolar ridge preservation, but this aspect has largely been ignored. We, therefore, hypothesize that biomimetic-charged BTO/P(VDF-TrFE) membranes can accelerate alveolar ridge regeneration and enhance ARP efficacy, *via* restoration of the electrical microenvironment within the extraction socket, as illustrated in Scheme 1.

Experimental

Fabrication of BTO/P(VDF-TrFE) composite membranes

A solution casting method was used to fabricate BTO/P(VDF-TrFE) composite membranes (Fig. 1a) based on our previous study.[14] Briefly, BTO nanoparticles (99.9%, average particle size of 100 nm, Alfa Aesar, USA) were first modified by dispersion in 0.01 mol L^{-1} dopamine hydrochloride (99% w/v, Alfa Aesar). Then the dopamine-modified BTO nanoparticles and P(VDF-TrFE) co-polymer powders (65/35 mol% VDF/TrFE, Arkema, France) were proportionally dispersed in the *N*,*N*-dimethylformamide (DMF) solvent by ultrasonication and stirring to form a stable suspension. The suspension was then cast into membranes and dried at 55 °C for solvent volatilization. The nanocomposite membranes were then treated with corona poling under a DC

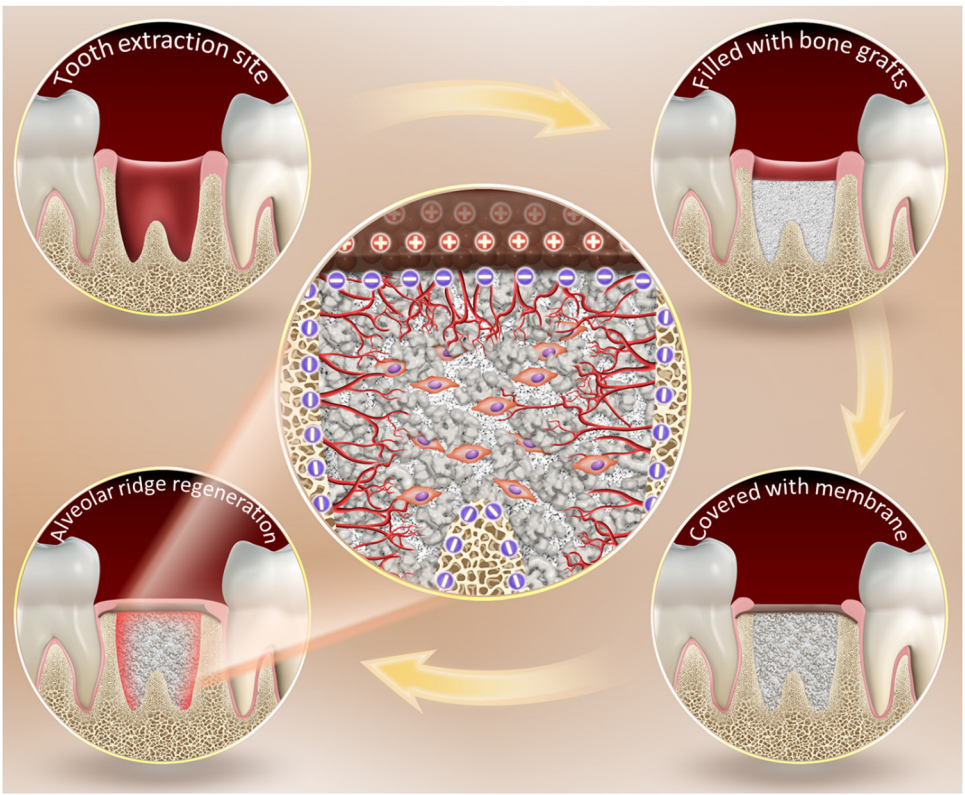

Scheme 1 Illustration of the therapeutic benefits of the restoring electrical microenvironment of the dental alveolar socket *via* implantation of the biomimetic charged BTO/P(VDF-TrFE) nanocomposite membrane at the alveolar ridge. The polarized charges are generated on the surfaces of BTO/P(VDF-TrFE) nanocomposite membranes after corona poling treatment. When the membrane was implanted as a barrier membrane to cover tooth extraction sites filled with bone grafts, the electrical microenvironment is stably maintained, resulting in enhanced neovascularization and rapid bone regeneration, which consequently enhanced buccal alveolar bone regeneration and maturation.

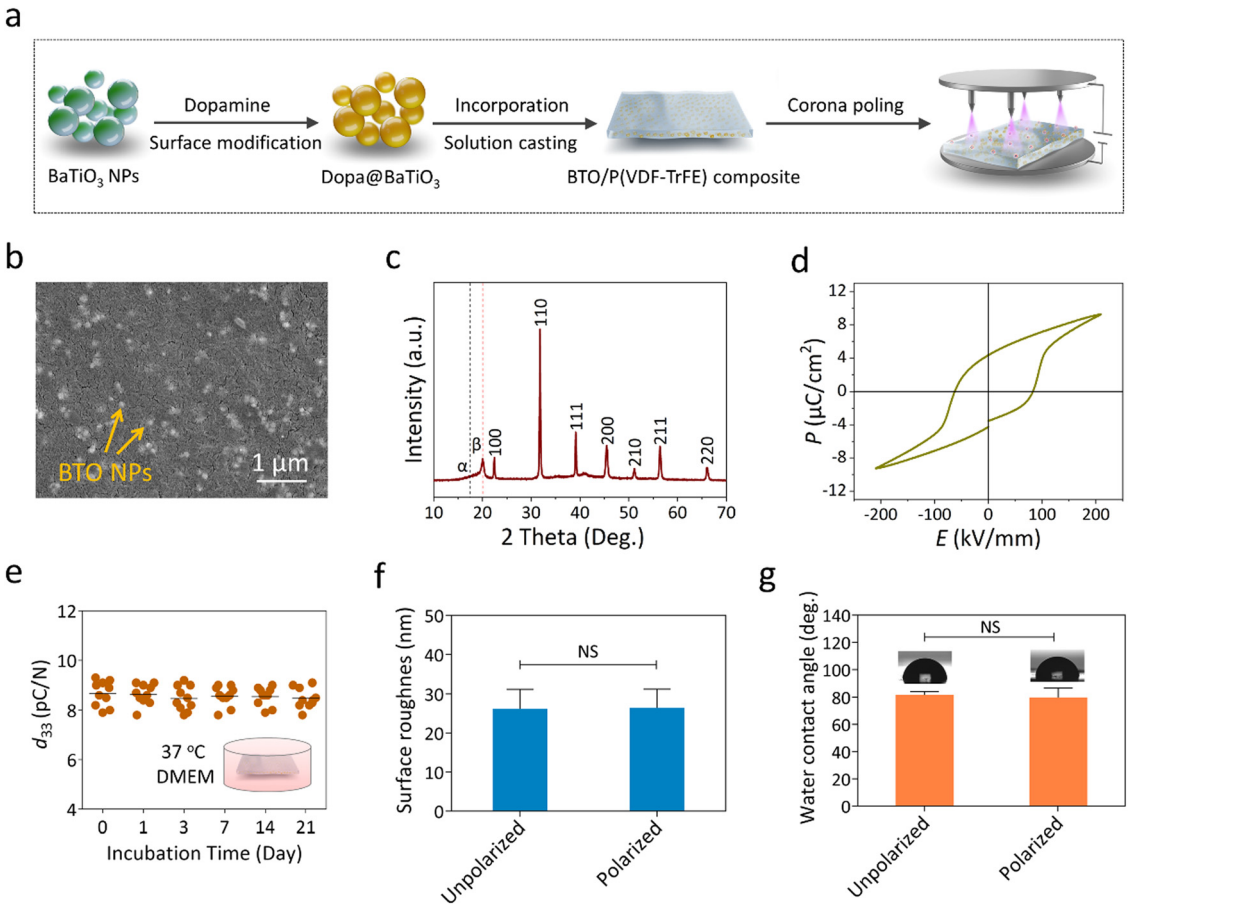

Fig. 1 Characterization of the physicochemical properties of the BTO/P(VDF-TrFE) membrane. (a) Schematic diagram of the charged BTO/P(VDF-TrFE) nanocomposite membrane fabrication process. (b) Representative SEM image of the surface morphology of charged nanocomposite membranes. (c) The X-ray diffraction patterns of charged membranes. (d) The hysteresis loops of BTO/P(VDF-TrFE) nanocomposite membranes. (e) The piezoelectric coefficient (d_{33}) values of the charged membranes after immersion in a serum-free cell culture medium for different time durations. (e) The surface roughness of BTO/P(VDF-TrFE) membranes was examined by atomic force microscopy, before and after corona poling treatment. (f) The water contact angles of BTO/P(VDF-TrFE) composite membranes before and after corona poling treatment. (Yellow arrows denote the BTO nanoparticles. NS denotes no statistical significance).

field of 1 kV mm^{-1} at room temperature. The thickness of the nanocomposite membranes was about 30–50 μm.

Characterization of the BTO/P(VDF-TrFE) composite membranes

The morphological characteristics and internal structures of the polarized membranes were examined by field emission scanning electron microscopy (S-4800, HITACHI, Japan). X-Ray diffraction spectroscopy (XRD, Rigaku D/max 2500 VB2t/PC, Japan) was used to characterize the ferroelectric properties of the membrane. The polarization–electric field (P–E) loops were measured using a commercially-available ferroelectric analyzer test setup (TF1000, aixACCT Systems GmbH, Germany) at a frequency of 10 Hz. The electrical properties of the nanocomposite membranes after corona poling were measured as the piezoelectric coefficient (d_{33}) using a piezoelectric coefficient meter (ZJ-3AN, IACAS, China). For electrical stability evaluation, the polarized nanocomposite membranes were rinsed with ddH2O, after immersion in a serum-free cell culture medium for 1, 3, 7, 14, and 21 days, to evaluate changes in piezoelectric coefficients. The surface roughness of the membranes was examined by atomic force microscopy (AFM; Dimension Icon, Bruker, USA) in the contact mode, and the surface wettability of the samples was assessed by measuring the water contact angle with a video contact angle instrument (JC2000C1, Shanghai Glory Numeral Technique & Device Co, Ltd, China).

Animal experimental procedures

Eight 2-year-old male mini-pigs (BA-MA, Guangxi) were maintained under specific pathogen-free conditions. The experimental protocol was approved by the Animal Care and Use Committee of the Beijing Strong Century Minipigs Breeding Base. Clinical tooth extraction site models were created on each side of the posterior regions of the maxilla and mandibular of the 8 minipigs by removing the second premolars (P2) and the fourth premolars (P4) of each mini-pig (Fig. 2a). Following the principle of minimally invasive surgery (Fig. 2b), the animals received dental prophylaxis and all surgical sites were swabbed

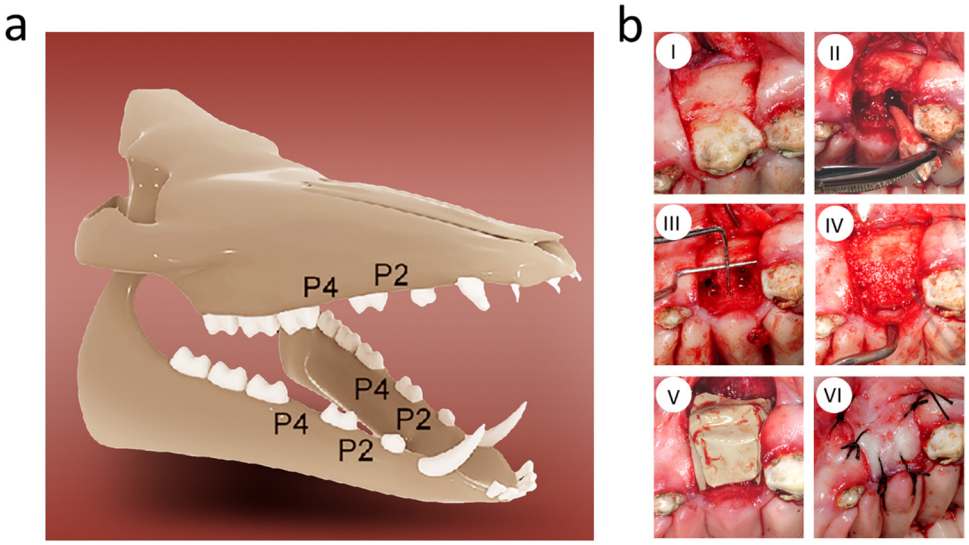

Fig. 2 Schematic illustration of extraction site positions in mini-pigs and surgery record photographs. (a) Schematic illustration of the positions of tooth extraction sites, all being either the second premolars (P2) or the forth premolars (P4) of each mini-pig. (b) Surgery record photographs. I. full thickness mucoperiosteal flaps were raised for extraction with two vertical releasing incisions; II. the tooth being extracted with clinical trauma; III. the measurement of each extraction site; IV. intact socket filled with Bio-Oss®; V. Extraction site was covered with the BTO/P(VDF-TrFE) membrane; VI. primary flap closure was achieved.

with 0.12% (w/v) chlorhexidine gluconate solution before surgery. Following intravenous administration of tiletamine hydrochloride and zolazepam hydrochloride (Zoletil® 50, 5 mg kg^{-1}) and xylazine hydrochloride (2.2 mg kg^{-1}), with the maintenance dose being 1/3 to 1/2 of the initial dose, administered every two hours, local anesthesia was achieved using Primacaine. Full thickness mucoperiosteal flaps were raised for extraction with two vertical releasing incisions and the tooth was separated and extracted with minimal trauma. The granulated tissue was removed and the socket was irrigated with sterile saline. Bio-Oss® (Geistlich Pharma, Switzerland) was then placed into the sockets after measurements were made on each extraction site, followed by covering with the corresponding membranes. Then the sites were sutured. To prevent infection, the mini-pigs were injected with 1 g of cefazolin before the operation and 0.5 g of cefazolin twice a day for three days. The 8 mini-pigs were randomly allocated into two groups, based on the culling time points (3 months and 6 months after surgery). The 32 extraction sites of the 4 mini-pigs within each corresponding timepoint of culling were randomly assigned to four treatment groups as follows: (1) untreated group: intact socket unfilled and uncovered (Blank Control, n = 8), (2) polarized group: intact socket filled with Bio-Oss® and covered with a charged BTO/P(VDF-TrFE) membrane (test group, n = 8), (3) unpolarized group: intact socket filled with Bio-Oss® and covered with non-charged BTO/P(VDF-TrFE) membranes (negative Control, n = 8) and (4) PTFE group: intact socket filled with Bio-Oss® and covered with the PTFE membrane (Cytoplast® TXT-200, Osteogenics Biomedical, Inc, USA) (Positive Control, n = 8).

Cone beam computed tomography (CBCT) analysis

CBCT scanning was first performed one week after surgery, and then at 3 months and 6 months post-surgery with corresponding mini-pigs, according to the culling timepoint (Fig. 3a). To standardize radiographic measurements,[16–18] two sets of DICOM (Digital Imaging and Communications in Medicine) data sets were generated and transferred to a volumetric imaging software (Mimics 17.0, Belgium), in which three-dimensional reconstruction and image analyses were performed (Fig. 4a). After superimposition, the two data sets were aligned and manually checked for alignment. We established a reproducible and precise protocol to measure the changes of horizontal and vertical bone loss between one week after surgery, 3 months and 6 months post-surgery, according to the culling timepoint at the same extraction site. Measurements were made at the following three coronal sections, (1) the central-buccal height (CBH) resorption, (2) the central-lingual height (CLH) resorption, (3) horizontal width resorption was calculated at 1 mm (HWB, −1 mm), 3 mm (HWB, −3 mm), and 5 mm (HWB, −5 mm) below the middle buccal crest (Fig. 4b). All measurement data were averaged from 3 replicate readings by the same tester.

Micro-CT analysis

After 3 months or 6 months post-surgery, the samples were harvested and fixed in 4% (w/v) paraformaldehyde for 24 h at 4 °C, and the specimens were then examined using micro-CT scanning as previously described.[19,20] Files were reconstructed using a modified Feldkamp algorithm, which was created using a microtomographic analysis software (Tomo NT, Skyscan, Belgium). Bone morphometric analyses, including the calculation of bone volume (BV/TV) and bone mineral density (BMD), were carried out manually on the same volume of interest (VOI), with dimensions of 3 × 3 × 5 mm^3, below the canal orifice of each extraction socket root. 3D and 2D images were constructed from the micro-CT scanning data.

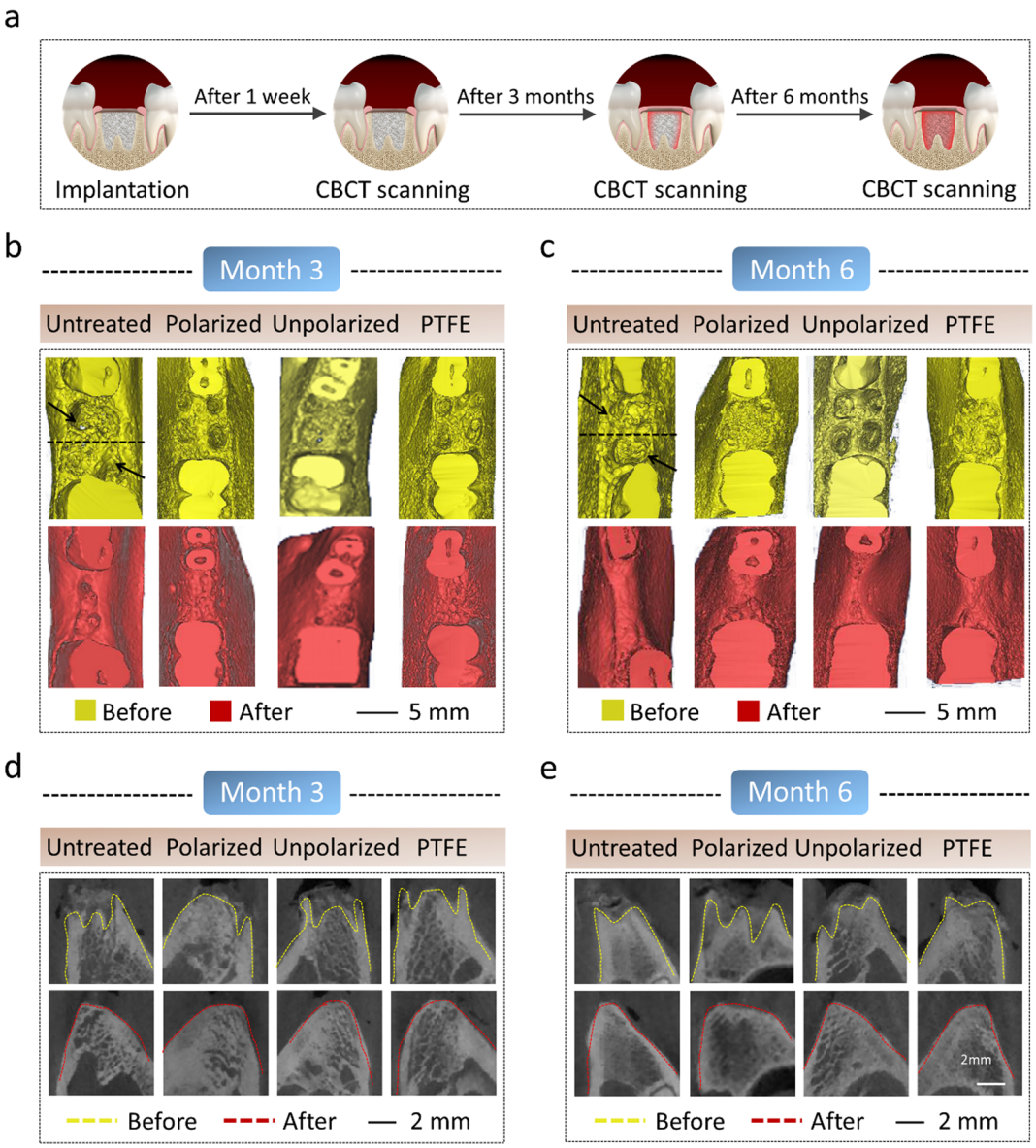

Fig. 3 Qualitative analyses of the therapeutic effects of restoring the electrical microenvironment on alveolar bone preservation and three-dimensional shape maintenance by CBCT. (a) Schematic illustration of the CBCT detection time-points. (b) Representative three-dimensional (3D) CBCT imaging (the occlusal view) of the tooth extraction sockets after implantation for 3 months. (c) Representative three-dimensional (3D) CBCT imaging (the occlusal view) of the tooth extraction sockets after implantation for 6 months. (d) Representative two-dimensional (2D) CBCT imaging (cross-sectional view) of tooth extraction sockets after implantation for 3 months. (e) Representative two-dimensional (2D) CBCT imaging (cross-sectional view) of tooth extraction sockets after implantation for 6 months. The yellow model was used as the reference and was created at 1 week after surgery (before), while the red model was created after 3 months or 6 months of healing (after). Black arrows denote the tooth extraction sockets. The dotted black lines represent the position of the 2D cross section at the center of the extraction sites.

Histological analysis

After immersion fixation in 4% (w/v) paraformaldehyde supplemented with 1% (w/v) calcium chloride, the hemi-mandibles were processed for the production of undecalcified ground sections. Decalcification and dehydration procedures were performed according to standard protocols; followed by embedment in paraffin; and sectioning in 5 μm thickness. Hematoxylin and eosin (H&E) staining and Masson's trichrome staining[21,22] were performed separately following the manufacturer's protocols. All slides were then imaged and analyzed using supporting software (Bioquant Osteo Bone Biology Research System, USA). Bone area analysis was carried out on the same region of interest (ROI), measuring the area of the buccal side (10×10 mm^2) below the middle alveolar crest.

Statistical analysis

All quantitative data were expressed as mean ± standard error of the mean (SEM). Statistical analyses were performed using the SPSS 19.0 software (IBM Corp, USA). Statistical differences were analyzed using Student's *t*-test for independent samples.

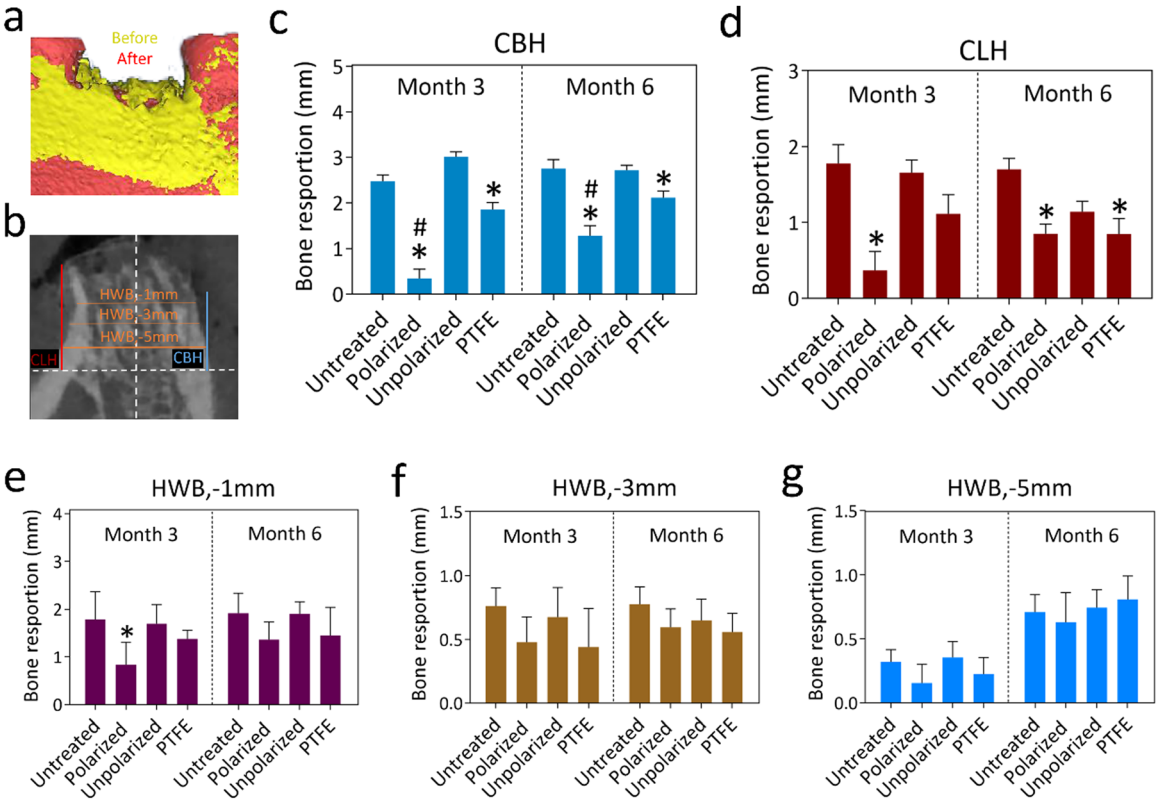

Fig. 4 Quantitative analyses of the therapeutic effects of restoring electrical microenvironment on alveolar bone preservation and three dimensional shape maintenance by CBCT. (a) The three-dimensional digital images of CBCT before and after healing. (b) A coronal section of the CBCT image at the center of a representative extraction site immediately after surgery. The central-buccal height (CBH). The central-lingual height (CLH). Horizontal width changes were calculated as the distance between two points at three levels, 1 mm (HWB, −1 mm), 3 mm (HWB, −3 mm), and 5 mm (HWB, −5 mm) apically to the central-buccal height (CBH). (c) The quantitative results of vertical resorption for CBH after implantation for 3 months and 6 months. (d) The quantitative results of vertical resorption for CLH after implantation for 3 months and 6 months. (e–g) The quantitative results of horizontal resorption after 3 months and 6 months healing. The yellow model was used as reference and was created at 1 week after surgery (Before), while the red model was created after 3 months or 6 months of healing (After). $^{*}p < 0.05$ compared to untreated. $^{\#}p < 0.05$ compared to PTFE.

$^{*}P < 0.05$ denotes a statistically significant difference compared with the untreated control, while $\#P < 0.05$ denotes a statistically significant difference compared with the PTFE group.

Results

Physicochemical characterization of BTO/P(VDF-TrFE) composite membranes

The SEM images showed that the membrane surface was smooth and flat (Fig. 1b), with the BTO NPs being evenly distributed throughout the polymer matrix (indicated by the yellow arrows). XRD patterns exhibiting typical BTO crystallization characteristics and polar β-phase were observed (Fig. 1c), which confirmed the characteristics of the ferroelectric ceramic BTO and ferroelectric polymer P(VDF-TrFE). Typical hysteresis loops were observed in the *P–E* curves (Fig. 1d), which showed the ferroelectric behavior of electrical polarization of the nanocomposite membrane. The d_{33} measurement results showed that the piezoelectric coefficient of the polarized nanocomposite membranes ($\sim$9.1 pC N^{-1}) was similar to the endogenous potential of human bone[23] and remained stable at about 97.8% of its original value, even after 21 days in a simulated physiological conditions (Fig. 1e). The quantitative characterization data suggested that there were no significant differences in surface roughness (Fig. 1f) and water contact angles (Fig. 1g) between the unpolarized and polarized membranes.

Therapeutic efficacy of restoration of the electrical microenvironment on vertical and horizontal alveolar ridge preservation

CBCT scanning of the tooth extraction sites was first performed one week after surgery, and then after 3 months or 6 months of healing. As shown in Fig. 3, the tooth extraction sites of the polarized group healed with the most optimal bone shape and most complete closure of the socket entrance after 3 and 6 months of healing, as compared with the other groups (Fig. 3b–e). This will not only be beneficial for the sustainable maintenance of the local electric environment, but will also be convenient for subsequent removal after the completion of bone healing.

After 3 months of healing, the changes in the buccal alveolar ridge height at the tooth extraction sites were observed and measured. Compared with the untreated (2.48 ± 0.14 mm) and unpolarized (3.01 ± 0.11 mm) groups, the absorption of buccal alveolar bone in the polarized (0.34 ± 0.21 mm) and

PTFE (1.85 ± 0.15 mm) groups were significantly reduced ($p < 0.05$), with the effect of the polarized group being better than that of the PTFE group ($p < 0.05$) (Fig. 4c). With regards to lingual alveolar ridge resorption, Fig. 4d showed that the resorption of lingual alveolar bone in the polarized group (0.37 ± 0.25 mm) was significantly less than that in the other three groups ($p < 0.05$). As shown in Fig. 4e–g, the horizontal width resorption was calculated at 1 mm (HWB, −1 mm) below the middle buccal crest, of which the polarized group (0.84 ± 0.24 mm) was significantly less than that in the other 3 groups ($p < 0.05$). With regards to horizontal width resorption at 3 mm (HWB, −3 mm), and 5 mm (HWB, −5 mm) below the middle buccal crest, there were no statistically significant differences between all the groups ($p > 0.05$), with resorption being lowest in the polarized group.

After 6 months of healing, a comparison with the untreated (2.76 ± 0.20 mm) and unpolarized (2.72 ± 0.11 mm) groups showed that the vertical resorption of buccal alveolar bone in the polarized (1.28 ± 0.22 mm) and PTFE (2.11 ± 0.15 mm) groups were significantly reduced ($p < 0.05$), with the effects observed in the PTFE (2.11 ± 0.15 mm) group being second only to the polarized group ($p < 0.05$) (Fig. 4c). As seen in Fig. 4d, the vertical resorption of lingual alveolar bone in the polarized (0.84 ± 0.13 mm) and PTFE (0.85 ± 0.20 mm) groups were also significantly reduced, as compared to the untreated (1.70± 0.14 mm) and unpolarized (1.14 ± 0.14 mm) groups, with the resorption of the polarized group being less than that of the PTFE group, even though differences were not significantly different. Horizontal width resorption was calculated at 1 mm (HWB, −1 mm), 3 mm (HWB, −3 mm), and 5 mm (HWB, −5 mm) below the middle buccal crest after 6 months of healing. There were no significant differences among the four groups, but the resorption in the polarized group was less than the other groups (Fig. 4e–g).

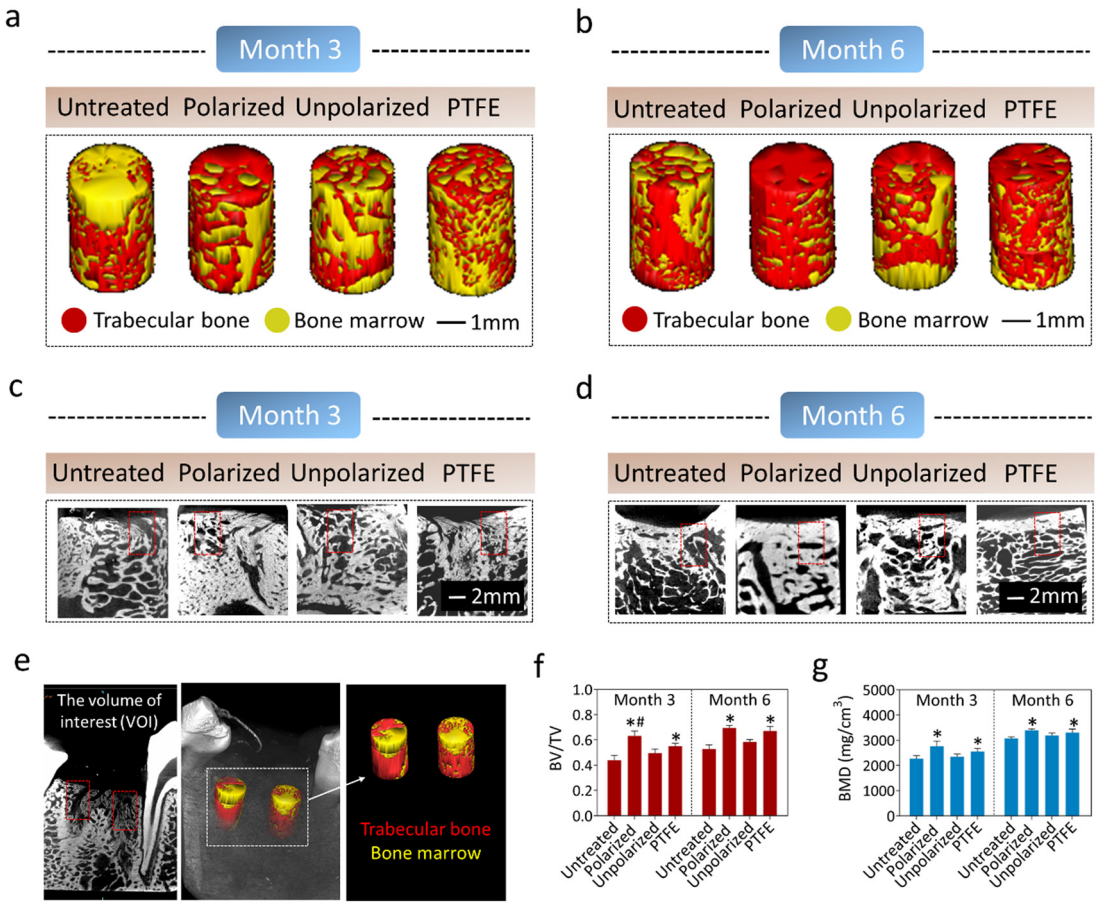

Fig. 5 Bone morphometric analyses (Micro-CT) of tooth extraction sockets after alveolar ridge preservation with restoration of electrical microenvironment. (a) Representative three-dimensional (3D) Micro-CT imaging of tooth extraction sockets after 3 months of healing. (b) Representative three-dimensional (3D) Micro-CT imaging of tooth extraction sockets after 6 months of healing. (c) Representative two-dimensional (2D) Micro-CT imaging of tooth extraction sockets after 3 months of healing. (d) Representative two-dimensional (2D) Micro-CT imaging of tooth extraction sockets after 6 months of healing. (e) The representative samples of Micro-CT analysis. The same volume of interest (VOI) was measured manually ($3 \times 3 \times 5$ mm^3) for each tooth extraction socket in the root. The red portion denotes trabecular bone, while the yellow portion denotes bone marrow-like tissue. The red dotted boxes denote the volume of interest (VOI) below the canal orifice of each tooth extraction socket root. (f) Quantitative analysis results of bone volume/tissue volume (BV/TV) after implantation for 3 months and 6 months. (g) Quantitative analysis results of bone mineral density (BMD) after implantation for 3 months and 6 months. *$p < 0.05$ compared to untreated. $^{\#}p < 0.05$ compared to PTFE.

The bone regeneration efficacy upon restoration of the electrical microenvironment in tooth extraction sockets

Micro-CT analysis showed that the restoration of the electrical microenvironment yielded a substantial increase in regenerated bone volume/tissue volume (BV/TV) and bone mineral density (BMD) (Fig. 5) within the tooth extraction socket roots.

After 3 months of healing, conspicuous regeneration of new bone with a stout trabecular bone structure ingrowth within the extraction socket was observed in the polarized group, whereas more bone marrow-like tissues filled the extraction sockets in the other three groups (Fig. 5a). Interestingly, dense regenerated alveolar ridge structures appeared in the polarized group, as can be observed from the 2-D images (Fig. 5c), while the other three groups displayed a certain degree of collapse of the alveolar ridge. This difference might be attributed to the fact that the charged membrane surface can induce osteogenic differentiation and rapid accumulation of stem cells *in vivo*. Quantitatively, the BV/TV value in the polarized (0.63 ± 0.02) groups was higher than those in the untreated (0.44 ± 0.02), unpolarized (0.50 ± 0.02) and PTFE groups (0.55 ± 0.01) ($p < 0.05$), with that of the polarized group being higher than the PTFE group ($p < 0.05$) (Fig. 5f). The BMD in the polarized (2757.76 ± 93.81 mg cm^{-3}) group was higher than that in the untreated (2263.24 ± 62.26 mg cm^{-3}) and unpolarized (2342.31 ± 55.31 mg cm^{-3}) groups ($p < 0.05$), while being just slightly higher than the PTFE group (2549.23 ± 66.66 mg cm^{-3}) (Fig. 5g).

After 6 months of healing, it can be observed that almost completely newly-regenerated bone tissue occupied the extraction socket in the polarized group, and that the trabecular structure of the newly regenerated bone becomes denser and more calcified, while the other three groups still had some bone marrow-like tissue filling the extraction socket (Fig. 5b). From the 2-D images (Fig. 5d), it can be observed that the alveolar ridge regeneration structure has become denser in the polarized group, while the other three groups still appeared to have looser structures. Quantitatively, the BV/TV values of the polarized (0.69 ± 0.01) and PTFE (0.67 ± 0.02) groups were significantly higher than the untreated (0.53 ± 0.02) and unpolarized (0.58 ± 0.01) groups ($p < 0.05$), with that of the polarized group being just slightly higher than the PTFE group (Fig. 5f). The BMD in the polarized (3398.81 ± 31.98 mg cm^{-3}) and PTFE (3304.31 ± 70.23 mg cm^{-3}) groups were also significantly higher than the untreated (3073.96 ± 38.60 mg cm^{-3}) and unpolarized (3192.06 ± 56.26 mg cm^{-3}) groups ($p < 0.05$), with that of the polarized group being just slightly higher than the PTFE group (Fig. 5g).

The augmentation effects of restoration of the electrical microenvironment on the buccal plate of the tooth extraction socket

The histological analysis further revealed that the restoration of the electrical microenviroment was conducive to alveolar ridge preservation and alveolar bone augmentation. No adverse reaction was observed during the entire bone healing process.

After 3 months of healing, the H–E staining results showed that the alveolar ridge dimensions in the polarized group were significantly better compared to that of the other three groups, although the PTFE group also had improved alveolar ridge dimensions (Fig. 6a). Furthermore, contiguous newly-regenerated bone filled the extraction socket of the polarized group, as can be seen from the local enlarged images, with the lamellar bone in the crestal and buccal portions of the extraction socket being relatively well formed (Fig. 6b). In addition, the alveolar bone center exhibited a homogeneous woven bone structure, while the other three groups did not form any obvious lamellar bones within the buccal alveolar ridge, with just a woven bone structure being observed (Fig. 6b). Masson staining displayed similar phenomena and trends (Fig. 6c and d). Quantitatively, there were higher percentages of bone areas within the regenerated buccal alveolar bone of the polarized group (62%) *versus* PTFE (51.67%) groups ($p < 0.05$) (Fig. S1a, ESI†).

After 6 months of healing, better 3D shapes of the buccal plate of the alveolar bone were observed in the polarized group *versus* PTFE group, with the therapeutic effects of the polarized group being obviously the best (Fig. 7a). Furthermore, the extraction socket was filled with newly-regenerated bone that became partially mature in the polarized group, as can be seen from the local enlarged images (Fig. 7b). Also, the lamellar bone in the crestal and buccal portions of the extraction socket became thicker and more mature, as seen from the Masson staining images (Fig. 7c and d). However, it was observed that partially immature new bone continued to grow into the extraction socket in the other groups (Fig. 7c and d). This was confirmed by quantitative analyses (Fig. S1b, ESI†), which showed that the polarized group (62.33%) displayed a much higher percentage of the bone area of the buccal plate of alveolar bone than in the untreated (41.33%) and unpolarized (42.33%) groups ($p < 0.05$), but was just slightly higher than the PTFE group (53.33%). These results thus indicated that restoring the electrical microenvironment enhanced the preservation and augmentation of the buccal plate, and significantly promoted the remodeling and maturation of the tooth extraction sites, thus maintaining the three-dimensional shape.

Preclinical evaluation of the sub-chronic systemic toxicity of the electroactive membranes

Additionally, we also carried out long-term evaluation of the preclinical sub-chronic systemic toxicity of the electroactive membranes according to the protocol outlined by international standard ISO 10993-11. After three months of subcutaneous implantation of electroactive nanocomposite membranes in rats, no apparent toxicity was observed throughout the study period. All rats were weighed once every week. The body weight in each group increased over time. There was no statistically significant change in body weight between the electroactive BTO/P(VDF-TrFE) membrane group *versus* normal control group (Fig. S3, ESI†). The histopathological analyses of the liver, brain, thyroid, heart, lungs, thymus, intestine, kidneys, pancreas, adrenal gland, spleen and salivary gland revealed normal tissue architecture (Fig. S2, ESI†). After weighing each organ and calculating the ratio of the organ to body weight, there was observed to be no significant changes in the organ

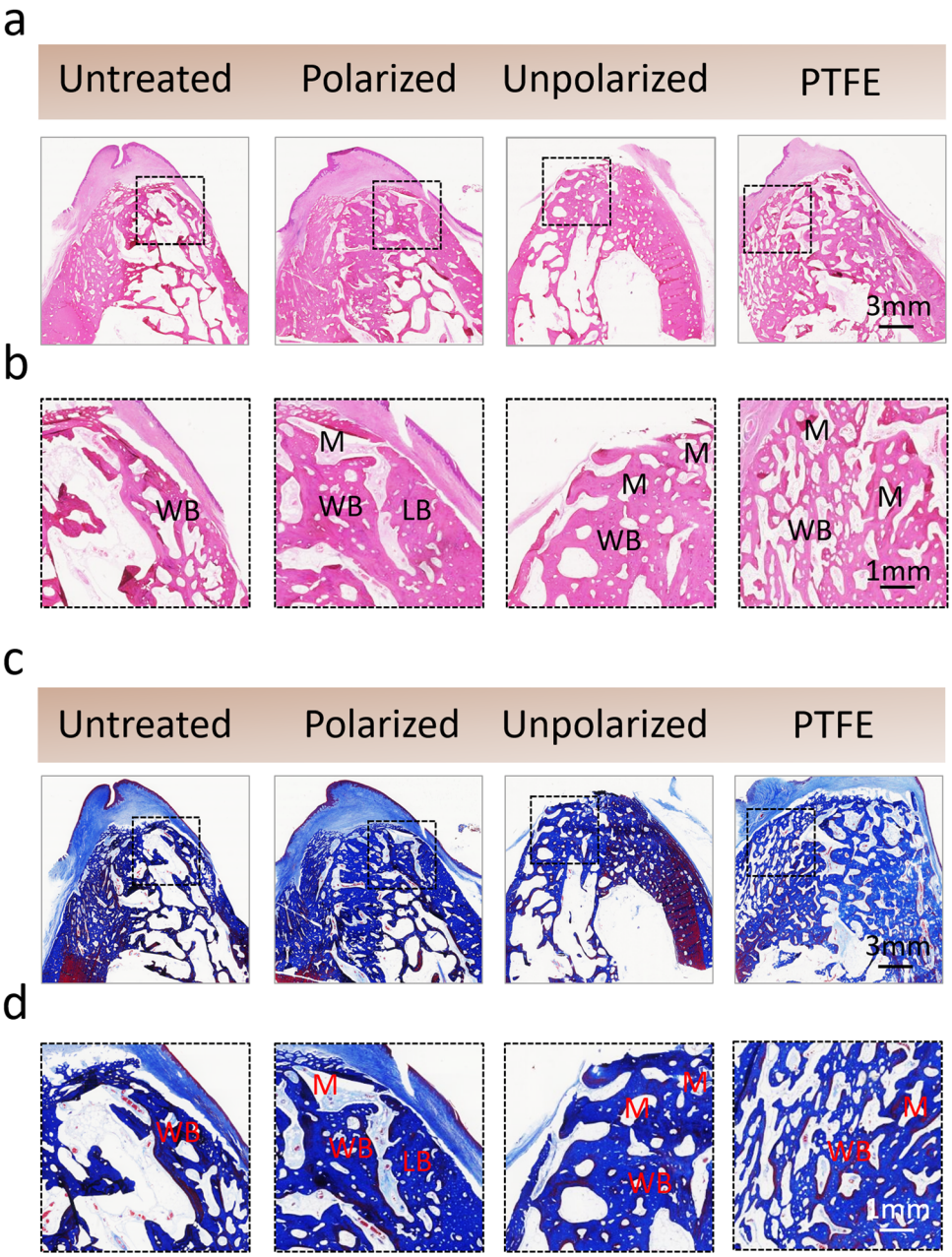

Fig. 6 Histological analyses of the preservation and regeneration of the alveolar ridge after restoring the electrical microenvironment for 3 months. (a) Representative H&E staining images of the alveolar ridge after 3 months of healing. (b) High magnification view of the boxed area in (a). (c) Representative Masson's trichrome staining images of the alveolar ridge after 3 months of healing. (d) High-magnification view of the boxed area in (c). LB, lamellar bone; WB, woven bone; M, bone grafts materials.

weight ratio between the BTO/P(VDF-TrFE) group *versus* the blank control group (Table S1, ESI†). Additionally, the rats were sacrificed and their blood was collected from the abdominal aorta for biochemical analyses. There were no significant changes in the total protein (TP), albumin (ALB), alkaline phosphatase (ALP), aspartate aminotransferase (AST), creatinine (CRE), blood glucose (GLU), alanine aminotransferase (ALT), total bilirubin (TBIL), triglyceride (TG), calcium (Ca), inorganic phosphorus (IP), urea (UREA) and cholesterol (CHO) levels between the electroactive BTO/P(VDF-TrFE) membrane group *versus* the normal control group (Table S2, ESI†). The blood was also collected from the abdominal aorta for cytological examination. There were no significant changes in the White blood cells (WBC), albumin (ALB), hemoglobin (HGB), hematocrit (HCT), platelet (PLT), activated partial thromboplastin time (APTT), prothrombin time (PT), International normalized ratio (INR) and prothrombin activity (PTA) between the BTO/P(VDF-TrFE) group *versus* blank control group (Table S3, ESI†). This rigorous preclinical long-term evaluation thus provides validation and support for safety

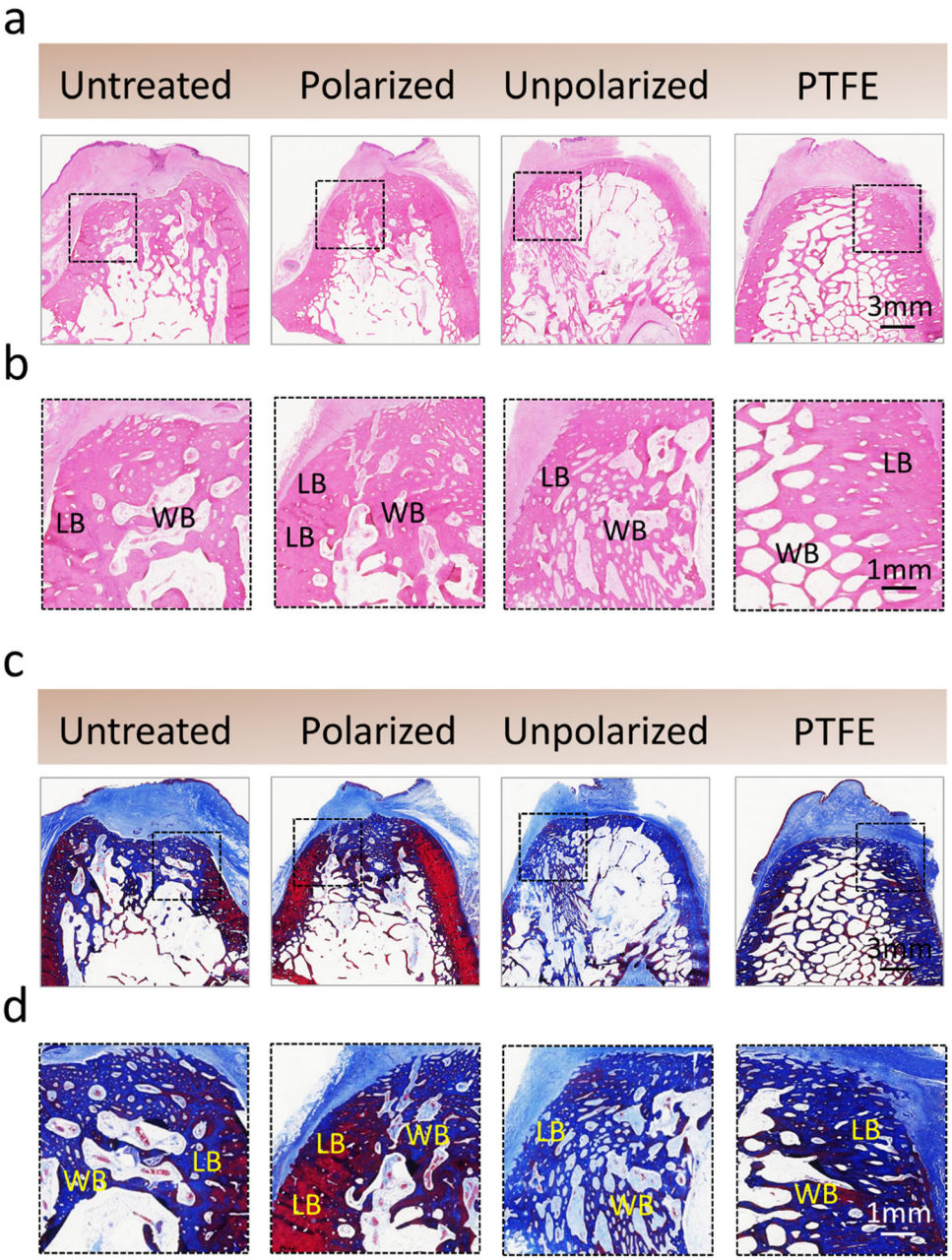

Fig. 7 Histological analyses of the preservation and regeneration of the alveolar ridge after restoring the electrical microenvironment for 6 months. (a) Representative H&E staining images of the alveolar ridge after 6 months of healing. (b) High magnification view of the boxed area in (a). (c) Representative Masson's trichrome staining images of the alveolar ridge after 6 months of healing. (d) High-magnification view of the boxed area in (c). LB, lamellar bone; WB, woven bone.

consideration of this electroactive membrane material in future clinical applications.

Discussion

The major drawbacks of commonly-used non-resorbable membranes for alveolar ridge preservation are the lack of osteoinductivity and adherence to newly regenerated bone.[4,24] The impact of the electrical microenvironment of the alveolar bone within the extraction socket on alveolar ridge preservation has largely been ignored. Hence, this study focused on the therapeutic efficacy of restoring the electrical microenvironment in the dental alveolar socket by implantation of a charged barrier membrane material for alveolar ridge preservation in a translational large animal model. Polarized ferroelectric BTO/P(VDF-TrFE) composite membranes had been demonstrated in our previous studies[14,15] to possess osteoinductive properties by restoring the electrical microenvironment of bone defects, as well as exhibiting much less adherence, possibly due to its

relatively low surface wettability (Fig. 2g). This could in turn facilitate easier removal of the implanted membrane after healing, thereby avoiding inflammation and other side effects of residual materials.

Adequate bone height and width could facilitate an ideal three-dimensional location of implant placement, subsequently resulting in optimal long-term functional and esthetic outcomes.[2] The key parameters for evaluating the efficacy of implanted barrier membranes in ARP applications are the vertical and horizontal alveolar bone volume. In this study, the results of CBCT analysis showed that both vertical and horizontal alveolar bone volume changes at the tooth extraction sites of the polarized BTO/P(VDF-TrFE) membrane group were significantly reduced, particularly at 3 months post-surgery (Fig. 3 and 4). This maintenance of alveolar bone volume may be beneficial for maintaining the three-dimensional shape of alveolar bone at the tooth extraction sites, which could in turn provide adequate implant space to better accommodate dental implant prostheses. Different therapeutic interventions (ridge preservation techniques) utilizing either bone replacement grafts or barrier membranes have been evaluated for their efficacy in mitigating against resorption, and have demonstrated partial efficacy in preserving the vertical and horizontal dimensions of the residual alveolar buccal bone crest.[25,26] Our results thus demonstrated that restoration of the electrical microenvironment in dental alveolar socket recapitulated by the polarized BTO/P(VDF-TrFE) membrane may exert a profound effect on preventing vertical and horizontal alveolar bone resorption for ARP therapy.

The results of the micro-CT analysis (Fig. 6) showed that the polarized BTO/P(VDF-TrFE) membrane promoted greater BV/TV and higher BMD at not only 3 months, but also at 6 months of healing, thus indicating that the polarized group yielded the best quality of regenerated bone. Bone quality profoundly affects the healing and long-term stability of the implant. Significantly higher rates of implant failure have been reported upon placement of implants in the bone of poor quality,[27,28] due to lower primary stability during operation[29] The smaller bone to implant contact area of implants placed in poor quality bone, often results in a higher loosening rate of implants during long-term use after rehabilitation.[30] Our results thus indicated that improved quality of the regenerated bone within the tooth socket of the polarized group could benefit the osseointegration quality of subsequent implants.

Aesthetic outcome and absorption of the implant labial bone plate, which is the most important cause of implant failure, are highly dependent on the thickness and quality of the buccal bone plate in the alveolar crest.[31,32] Previous studies demonstrated that aesthetic outcomes of dental implants depend to a large extent on the thickness of the buccal bone, as the most important parameter.[33,34] It must be noted that the dimensional reductions are greater in the buccal bone than that in the lingual bone after tooth extraction.[35,36] Hence better protection of the buccal plate becomes a key priority during ARP. The histological results showed that the restoration of the electrical microenvironment could maintain buccal plate thickness, at both 3 months and 6 months post-surgery (Fig. 6 and 7). This thus indicates that ARP with the biomimetic polarized BTO/P(VDF-TrFE) membrane is conducive to achieving better aesthetics and longer implant lifespan.

The implantable membrane was utilized as a barrier to provide a conducive microenvironment for promoting high osteogenic activity and encouraging recruitment of osteoprogenitors within the defect,[37] as well as for enhancing mechanical and anti-degradation properties.[38,39] In this study, the observed positive alveolar ridge preservation effects of the polarized *versus* PTFE group might be attributed to the membrane surface charge restoring the electrical microenvironment in the dental alveolar socket, thereby enhancing osteoblast activity and bone regeneration, as demonstrated in our previous studies.[14,15] Our results are also consistent with other studies which reported that polarized BTO/P(VDF-TrFE) membrane enhanced osteoblast differentiation and promoted bone defect healing in animals with osteoporosis-like symptoms.[40,41] Furthermore, the ability to consistently maintain high quality bone regeneration throughout the healing period in the polarized group may also be attributed to the structural integrity of the polarized nanocomposite membrane, which enables sustainable maintenance of the local electrical microenvironment. Our results thus imply that the restoration of the electrical microenvironment could significantly accelerate alveolar ridge preservation, which might exert a positive effect on promoting implant osseointegration.

Conclusions

In this study, the concept of restoring the electrical microenvironment to improve the effects of alveolar ridge preservation (ARP) was investigated in a mini-pig preclinical model. The restoration of the electrical microenvironment in dental alveolar socket recapitulated by the polarized BTO/P(VDF-TrFE) membrane could effectively mitigate against alveolar ridge resorption and enhance alveolar bone regeneration, when utilized synergistically with bone grafts, thus making it an innovative strategy for enhancing the clinical efficacy of ARP treatment for subsequent implant placement. Therefore, the clinical application value of the biomimetic polarized BTO/P(VDF-TrFE) composite membrane should not be underestimated, which could be expected to open up a new avenue for implant dentistry.

Author contributions

Y. P. L., Y. Z. M., Y. Y. B, Y. J. W. and J. Q. W. wrote the original manuscript, performed the fabrication and characterization of materials, histological analysis and interpretation, radiographic analysis and interpretation, sub-chronic systemic toxicity evaluation, and image preparation. B. C. H. supported animal study planning and performance, and revised the manuscript. J. Q. W. supported histological analysis and interpretation, and revised the manuscript. X. J. provided support in histological analysis and interpretation, and radiographic analysis and interpretation. X. H. Z., X. N. Z., M. G. and X. L. D.

were responsible for the study design and concept, supervised the study performance, evaluation, and manuscript writing, raised external funds and revised the manuscript.

Conflicts of interest

The authors declare that they have no competing interests.

Acknowledgements

This work was supported by the National Key Research and Development Program of China (2021YFB3800800, 2021YFC2400400, and 2022YFC2401803), the National Natural Science Foundation of China (82022016, 52273258, 82221003, 81991505, 32200658, and 51973004), the Beijing Municipal Natural Science Foundation (7222226), Peking University School of Stomatology National Clinical Key Discipline Construction Project (PKUSSNKP-T202101), National Program for Multidisciplinary Cooperative Treatment on Major Diseases (PKUSSNMP-202002) and the Natural Science Foundation of Hunan Province (2019JJ40400).

References

1 V. Lekovic, E. B. Kenney, M. Weinlaender, T. Han, P. Klokkevold, M. Nedic and M. Orsini, A bone regenerative approach to alveolar ridge maintenance following tooth extraction. Report of 10 cases, *J. Periodontol.*, 1997, **68**, 563–570.

2 F. Vignoletti and I. Abrahamsson, Quality of reporting of experimental research in implant dentistry. Critical aspects in design, outcome assessment and model validation, *J. Clin. Periodontol.*, 2012, **39**(Suppl 12), 6–27.

3 V. De Risi, M. Clementini, G. Vittorini, A. Mannocci and M. De Sanctis, Alveolar ridge preservation techniques: a systematic review and meta-analysis of histological and histomorphometrical data, *Clin. Oral. Implants Res.*, 2015, **26**, 50–68.

4 G. Avila-Ortiz, L. Chambrone and F. Vignoletti, Effect of alveolar ridge preservation interventions following tooth extraction: A systematic review and meta-analysis, *J. Clin. Periodontol.*, 2019, **46**(Suppl 21), 195–223.

5 V. Nguyen, N. von Krockow, J. Pouchet and P. M. Weigl, Periosteal Inhibition Technique for Alveolar Ridge Preservation as It Applies to Implant Therapy, *Int. J. Periodontics Restor. Dent.*, 2019, **39**, 737–744.

6 P. Bunyaratavej and H. L. Wang, Collagen membranes: a review, *J. Periodontol.*, 2001, **72**, 215–229.

7 D. Mandarino, D. Luz, V. Moraschini, D. M. Rodrigues and E. S. P. Barboza, Alveolar ridge preservation using a non-resorbable membrane: randomized clinical trial with biomolecular analysis, *Int. J. Oral Maxillofac. Surg.*, 2018, **47**, 1465–1473.

8 A. Cucchi, M. Sartori, A. Parrilli, N. N. Aldini, E. Vignudelli and G. Corinaldesi, Histological and histomorphometric analysis of bone tissue after guided bone regeneration with non-resorbable membranes vs resorbable membranes and titanium mesh, *Clin. Implant Dent. Relat. Res.*, 2019, **21**, 693–701.

9 F. P. Strietzel, P. Khongkhunthian, R. Khattiya, P. Patchanee and P. A. Reichart, Healing pattern of bone defects covered by different membrane types--a histologic study in the porcine mandible, *J. Biomed. Mater. Res., Part B*, 2006, **78**, 35–46.

10 M. Trobos, A. Juhlin, F. A. Shah, M. Hoffman, H. Sahlin and C. Dahlin, In vitro evaluation of barrier function against oral bacteria of dense and expanded polytetrafluoroethylene (PTFE) membranes for guided bone regeneration, *Clin. Implant Dent. Relat. Res.*, 2018, **20**, 738–748.

11 M. Zhao, B. Song, J. Pu, T. Wada, B. Reid, G. Tai, F. Wang, A. Guo, P. Walczysko, Y. Gu, T. Sasaki, A. Suzuki, J. V. Forrester, H. R. Bourne, P. N. Devreotes, C. D. McCaig and J. M. Penninger, Electrical signals control wound healing through phosphatidylinositol-3-OH kinase-gamma and PTEN, *Nature*, 2006, **442**, 457–460.

12 A. Huttenlocher and A. R. Horwitz, Wound healing with electric potential, *N. Engl. J. Med.*, 2007, **356**, 303–304.

13 C. Zhang, W. Liu, C. Cao, F. Zhang, Q. Tang, S. Ma, J. Zhao, L. Hu, Y. Shen and L. Chen, Modulating Surface Potential by Controlling the beta Phase Content in Poly(vinylidene fluoridetrifluoroethylene) Membranes Enhances Bone Regeneration, *Adv. Healthcare Mater.*, 2018, **7**, e1701466, DOI: **10.1002/adhm.201701466**.

14 X. Zhang, C. Zhang, Y. Lin, P. Hu, Y. Shen, K. Wang, S. Meng, Y. Chai, X. Dai, X. Liu, Y. Liu, X. Mo, C. Cao, S. Li, X. Deng and L. Chen, Nanocomposite Membranes Enhance Bone Regeneration Through Restoring Physiological Electric Microenvironment, *ACS Nano*, 2016, **10**, 7279–7286.

15 Y. Bai, X. Dai, Y. Yin, J. Wang, X. Sun, W. Liang, Y. Li, X. Deng and X. Zhang, Biomimetic piezoelectric nanocomposite membranes synergistically enhance osteogenesis of deproteinized bovine bone grafts, *Int. J. Nanomed.*, 2019, **14**, 3015–3026.

16 J. Hartlev, R. Spin-Neto, S. Schou, F. Isidor and S. E. Norholt, Cone beam computed tomography evaluation of staged lateral ridge augmentation using platelet-rich fibrin or resorbable collagen membranes in a randomized controlled clinical trial, *Clin. Oral. Implants Res.*, 2019, **30**, 277–284.

17 N. Saulacic, B. Schaller, F. Munoz, M. Fujioka-Kobayashi, E. Kobayashi, N. P. Lang and R. J. Miron, Recombinant human BMP9 (RhBMP9) in comparison with rhBMP2 for ridge augmentation following tooth extraction: An experimental study in the Beagle dog, *Clin. Oral. Implants Res.*, 2018, **29**, 1050–1059.

18 H. R. Hong, C. Y. Chen, D. M. Kim and E. E. Machtei, Ridge preservation procedures revisited: A randomized controlled trial to evaluate dimensional changes with two different surgical protocols, *J. Periodontol.*, 2019, **90**, 331–338.

19 C. H. Hammerle and R. E. Jung, Bone augmentation by means of barrier membranes, *Periodontol 2000*, 2003, **33**, 36–53.

20 L. Nie, H. Zhang, A. Ren, Y. Li, G. Fu, R. D. Cannon, P. Ji, X. Wu and S. Yang, Nano-hydroxyapatite mineralized silk fibroin porous scaffold for tooth extraction site preservation, *Dent. Mater.*, 2019, **35**, 1397–1407.

21 D. M. Kim, H. C. Lim, J. Y. Hong, S. I. Shin, J. H. Chung, Y. Herr and S. Y. Shin, Validity of Collagen Plugs for Ridge Preservation in a Canine Model, *Implant Dent.*, 2017, **26**, 892–898.

22 J. K. Cha, Y. K. Sun, M. J. Kim, M. Sanz and U. W. Jung, Antiresorptive effect of pamidronate on extraction socket wall in dogs, *Clin. Oral. Implants Res.*, 2018, **29**, 688–696.

23 X. Zhang, Y. Shen, Q. Zhang, L. Gu, Y. Hu, J. Du, Y. Lin and C. W. Nan, Ultrahigh energy density of polymer nanocomposites containing BaTiO3@TiO2 nanofibers by atomic-scale interface engineering, *Adv. Mater.*, 2015, **27**, 819–824.

24 N. MacBeth, A. Trullenque-Eriksson, N. Donos and N. Mardas, Hard and soft tissue changes following alveolar ridge preservation: a systematic review, *Clin. Oral. Implants Res.*, 2017, **28**, 982–1004.

25 W. L. Tan, T. L. Wong, M. C. Wong and N. P. Lang, A systematic review of post-extractional alveolar hard and soft tissue dimensional changes in humans, *Clin. Oral Implants. Res.*, 2012, **23**(Suppl 5), 1–21.

26 I. Rocchietta, M. Simion, M. Hoffmann, D. Trisciuoglio, M. Benigni and C. Dahlin, Vertical Bone Augmentation with an Autogenous Block or Particles in Combination with Guided Bone Regeneration: A Clinical and Histological Preliminary Study in Humans, *Clin. Implant Dent. Relat. Res.*, 2016, **18**, 19–29.

27 L. N. Teixeira, G. E. Crippa, R. Gimenes, M. A. Zaghete, P. T. de Oliveira, A. L. Rosa and M. M. Beloti, Response of human alveolar bone-derived cells to a novel poly(vinylidene fluoride-trifluoroethylene)/barium titanate membrane, *J. Mater. Sci.: Mater. Med.*, 2011, **22**, 151–158.

28 I. Sanz, M. Garcia-Gargallo, D. Herrera, C. Martin, E. Figuero and M. Sanz, Surgical protocols for early implant placement in post-extraction sockets: a systematic review, *Clin. Oral Implants Res.*, 2012, **23**(Suppl 5), 67–79.

29 M. M. Beloti, P. T. de Oliveira, R. Gimenes, M. A. Zaghete, M. J. Bertolini and A. L. Rosa, In vitro biocompatibility of a novel membrane of the composite poly(vinylidene-trifluoroethylene)/barium titanate, *J. Biomed. Mater. Res., Part A*, 2006, **79**, 282–288.

30 A. Barone, P. Toti, A. Piattelli, G. Iezzi, G. Derchi and U. Covani, Extraction socket healing in humans after ridge preservation techniques: comparison between flapless and flapped procedures in a randomized clinical trial, *J. Periodontol.*, 2014, **85**, 14–23.

31 L. A. Brownfield and R. L. Weltman, Ridge preservation with or without an osteoinductive allograft: a clinical, radiographic, micro-computed tomography, and histologic study evaluating dimensional changes and new bone formation of the alveolar ridge, *J. Periodontol.*, 2012, **83**, 581–589.

32 L. Zhao, T. Xu, W. Hu and K. H. Chung, Preservation and augmentation of molar extraction sites affected by severe bone defect due to advanced periodontitis: A prospective clinical trial, *Clin. Implant Dent. Relat. Res.*, 2018, **20**, 333–344.

33 J. M. Ten Heggeler, D. E. Slot and G. A. Van der Weijden, Effect of socket preservation therapies following tooth extraction in non-molar regions in humans: a systematic review, *Clin. Oral. Implants Res.*, 2011, **22**, 779–788.

34 F. Vignoletti, P. Matesanz, D. Rodrigo, E. Figuero, C. Martin and M. Sanz, Surgical protocols for ridge preservation after tooth extraction. A systematic review, *Clin. Oral Implants Res.*, 2012, **23**(Suppl 5), 22–38.

35 A. Barone, M. Ricci, P. Tonelli, S. Santini and U. Covani, Tissue changes of extraction sockets in humans: a comparison of spontaneous healing vs. ridge preservation with secondary soft tissue healing, *Clin. Oral. Implants Res.*, 2013, **24**, 1231–1237.

36 G. Vittorini Orgeas, M. Clementini, V. De Risi and M. de Sanctis, Surgical techniques for alveolar socket preservation: a systematic review, *Int. J. Oral Maxillofac. Implants*, 2013, **28**, 1049–1061.

37 A. Turri, I. Elgali, F. Vazirisani, A. Johansson, L. Emanuelsson, C. Dahlin, P. Thomsen and O. Omar, Guided bone regeneration is promoted by the molecular events in the membrane compartment, *Biomaterials*, 2016, **84**, 167–183.

38 A. L. G. Almeida, G. P. Freitas, H. B. Lopes, R. Gimenes, S. Siessere, L. G. Sousa, M. M. Beloti and A. L. Rosa, Effect of stem cells combined with a polymer/ceramic membrane on osteoporotic bone repair, *Braz. Oral Res.*, 2019, **33**, e079.

39 T. H. Leu, Y. Wei, Y. S. Hwua, X. J. Huang, J. T. Huang and R. J. Chung, Fabrication of PLLA/C3S composite membrane for the prevention of bone cement leakage, *Polymers*, 2019, **11**, 1971.

40 J. Li, X. Mou, J. Qiu, S. Wang, D. Wang, D. Sun, W. Guo, D. Li, A. Kumar, X. Yang, A. Li and H. Liu, Surface charge regulation of osteogenic differentiation of mesenchymal stem cell on polarized ferroelectric crystal substrate, *Adv. Healthcare Mater.*, 2015, **4**, 998–1003.

41 V. Marchesano, O. Gennari, L. Mecozzi, S. Grilli and P. Ferraro, Effects of lithium niobate polarization on cell adhesion and morphology, *ACS Appl. Mater. Interfaces*, 2015, **7**, 18113–18119.